Supporting Information

Highly Efficient Circularly Polarized Electroluminescence based on Chiral Manganese (II) Complexes

De-Hao Kong,[†] Yue Wu,[¶] Cui-Mi Shi,[†,§] Hao Zeng,[†,§] Liang-Jin Xu, [†,‡,§,*]
Zhong-Ning Chen [†,‡,§,*]

† *State Key Laboratory of Structural Chemistry, Fujian Institute of Research on the Structure of Matter, Chinese Academy of Sciences, Fuzhou 350002, China*

‡ *Fujian Science & Technology Innovation Laboratory for Optoelectronic Information of China, Fuzhou 350108, China*

§*University of Chinese Academy of Sciences, Beijing, 100039, China*

¶*School of Chemistry and Chemical Engineering, Liaocheng University, Liaocheng, Shandong,252000, China*

1.Raw materials and reagents:

R-2,2'-bis(diphenylphosphino)-1,1'-binaphthyl(R-Binap) / S-2,2'-bis(diphenylphosphino)-1,1'-binaphthyl (S- Binap) / Hydrogen peroxide (30%) (H_2O_2) / Manganese bromide anhydrous ($MnBr_2$).

Dichloromethane(CH_2Cl_2) /Methanol(CH_3OH) /Ethanol(C_2H_5OH) /Petroleum ether /Ethyl ether(Et_2O) /Deionized water /Anhydrous sodium sulfate(Na_2SO_4) /Silica gel chromatography column chromatography (SiO_2, 100-200 mesh).

2.Synthesis:

Synthesis of ligand S-Binapo: S-2,2'-bis(diphenylphosphino)-1,1'-binaphthyl (S-Binap) (2.00 g, 3.20 mmol) was dissolved in dichloromethane solvent (50 mL), and 30% of hydrogen peroxide (1.70 mL, 16.00 mmol) was slowly added to the above

solution at low temperature (around 0°C). Hydrogen peroxide (1.70 mL, 16.00 mmol) was slowly added to the above solution at low temperature (around 0°C) and then the reaction was stirred for 3 hours at room temperature. After the reaction was completed, 100 mL of deionized water was added to the reaction solution, and dichloromethane solvent was added in three times (3* 100 mL) to separate the organic and aqueous phases, respectively, to separate the organic and aqueous phases, and the organic phases from the three times of extraction were collected, and an appropriate amount of anhydrous sodium sulfate solids was added, and the solution was allowed to stand overnight to remove the water in the solution. After solid-liquid separation, the filtrate was collected, and the solvent in the filtrate was removed using a rotary evaporator, and then the crude product was separated and purified using silica gel chromatographic column method (the elution solvent was petroleum ether), and S-2,2'-bis(diphenyloxyphosphino)-1,1'-binaphthyl (S-Binapo) was obtained as a white solid of 2.05 g in 98% yield. 98%. 1H NMR δ H (400MHz, CDCl3) 6.79-6.80 (4H, m), 7.20-7.33 (10H, m), 7.35-7.46 (10H, m), 7.72 (4H, br dd,J= 7.9, 12.3Hz), 7.82 (2H, br d, J= 7.9 Hz), 7.86 (2H, dd, J=2.4, 7.9 Hz)。δ P (162 MHz, CDCl3) 29.2 (s, 2P)。

The ligand R-Binapo was synthesized in the same way as S-Binapo. R-2,2'-bis(diphenylphosphino)-1.1-binaphthyl (R-Binap) (3.20 g, 5.12 mmol) and 30% hydrogen peroxide (2.60 mL, 25.60 mmol) were synthesized to afford R-2,2'-bis(diphenylphosphino)-1,1'-binaphthyl (R-Binapo). 1H NMR δ H (400MHz, CDCl3) 6.76-6.82 (4H, m), 7.18-7.32 (10H, m), 7.34-7.45 (10H, m), 7.71 (4H, br dd,J= 7.9, 12.3Hz), 7.81 (2H, br d, J= 7.9 Hz), 7.85 (2H, dd, J=2.4, 7.9 Hz)。δ P (162 MHz, CDCl$_3$) 29.6 (s, 2P)。

Synthesis of the complex S-Mn(Binapo)Br$_2$: A 50 mL round bottom flask was charged with a mixture of 2,2'-bis(diphenylphosphino)-1,1'-binaphthyl (S-Binapo) (700 mg, 1.07 mmol) and manganese dibromide (229.78 mg, 1.07 mmol). They were dissolved in a mixture of dichloromethane and ethanol (6 mL each), and the above solutions were stirred at room temperature for 3 hours. At the end of the reaction, the above solution was transferred to a test tube, and ether was chosen as the poor solvent and slowly added to the upper layer of the test tube, which was sealed and stored for

about one week, and the formation of massive crystals was observed. ^{31}P NMR δ P (162 MHz, CDCl$_3$) 37.3 (s, 2P)。

R-Mn(Binapo)Br$_2$ was synthesized by the same route as S-Mn(Binapo)Br2. Massive crystals of R-Mn(Binapo)Br$_2$ were obtained from R-2,2'-bis(diphenylphosphino)-1,1'-binaphthyl (R- Binapo) (700 mg, 1.07 mmol) and manganese dibromide (229.78 mg, 1.07 mmol). ^{31}P NMR δ P (162 MHz, CDCl$_3$) 37.3 (s, 2P)。

3.Characterizations.

Photoluminescence (PL) Steady State Studies. PL properties, including emission and excitation spectra in solid state at room temperature, were measured on an FLS 1000 Edinburgh fluorescence spectrometer. In addition, PL quantum efficiency measurements were performed using the same light source with an additional integrating sphere by FLS 1000 Edinburgh fluorescence spectrometer. The PLQY was calculated by following equation (S1)：

$$\eta = \left(\int L_{direct} - \int L_{blank} \right) / \left(\int E_{without} - \int E_{direct} \right) \quad (S1)$$

where η is the photoluminescent quantum yield, L_{direct} is the complete emission spectrum of the sample collected by using the integrating sphere, L_{blank} is the emission spectrum of the blank sample, E_{direct} is the emission spectra of the excitation light, recorded with the sample in place, and $E_{without}$ is the emission spectrum of excitation light, recorded with the equipment blank in place. The part $\left(\int L_{direct} - \int L_{blank} \right)$ expresses the photons emitted by our sample, and $\left(\int E_{without} - \int E_{direct} \right)$ means the photons emitted by excitation light source. Time-resolved emission data were collected at room temperature using the FLS 1000 spectrofluorometer with a microsecond light source.

Study of chiral properties. The test of tablet compression samples was performed using a circular dichroism spectrometer of the instrument model MOS-450, with scanning range of 200-800 nm, wavelength accuracy of ± 0.1 nm, circular dichroism detection of 0.01 mdeg, and the baseline stability of less than 0.01 mdeg/hr, The

sampling frequency is 5 seconds/point, and the circular dichroism signal is obtained under the condition of a 150W xenon lamp with a light source. The characteristics of chiral optically active substances in the excited state were investigated using a circularly polarized fluorescence spectrometer with a model JASCO CPL-300, the detector was a photoelectron multiplier tube PMT, the scanning speed was set to 100 nm/min, and the D.I.T. was 1 sec, The properties of chiral optically active substances in the excited state were studied under the excitation of 350 nm under the excitation of a 150W air-cooled Hg-Xe lamp.

OLED device preparation. The OLED device structure was ITO/ PEDOT:PSS/ hybrid host material:TAPC/ complex S-Mn(Binapo)Br$_2$/ 2,6-DCzPPY/ TmPyPb/ LiF/ Al. The ITO glass substrate was cleaned in an ultrasonicator using de-ionized water for 30 min, and then ultrasonically cleaned using acetone and isopropanol in sequence for 30 min, respectively. The glass substrate was rinsed again with deionized water. The glass substrates were rinsed again with deionized water, dried, and then treated with UV ozone for 30 min. PEDOT:PSS was spin-coated onto the treated ITO substrates through a 0.22 pum filter at a rotational speed of 4800 r/min, and then annealed for 15 min at 130°C. The glass substrates were protected by nitrogen gas and annealed for 15 min at 130°C. The glass substrates were then cleaned with acetone and isopropanol. A CH$_2$Cl$_2$ solution (6 mg /mL) containing the mixed host material and the complex was spin-coated onto the PEDOT:PSS layer under nitrogen protection at 4000 r/min and annealed at 40°C for 15 minutes. It was then transferred to a vacuum chamber and the electron transport layer (TmPyPb), electron injection layer (LiF), and Al as cathode were deposited on ITO glass substrates with thicknesses of 50 nm, 1 nm, and 100 nm, respectively, by vapor deposition under vacuum conditions below 4x 10^{-4} Pa. The photovoltaic data, such as voltage-current density-brightness, were obtained on a Keithry 2400 light meter and calibrated silicon photodiodes were measured. Electroluminescence (EL) spectroscopy tests were performed on a HORIBA-Join-YonFluoroMax-4 spectrometer. All tests were performed directly in dry air.

The crystal filed calculation based on Tanabe-Sugano energy level diagram. In this work, the crystal field Dq and Racah B parameters are calculated by the

equations (1)-(3) listed below:

$${}^{6}A_1 (6S) \rightarrow {}^{4}A_1, {}^{4}E (G) = 10B + 5C \tag{1}$$

$${}^{6}A_1 (6S) \rightarrow {}^{4}E (D) = 17B + 5C \tag{2}$$

$${}^{6}A_1 (6S) \rightarrow {}^{4}T_2 (G) = -10Dq + 18B + 6C - (26B^2 /10Dq) \tag{3}$$

Notably, the corresponding absorption peaks of ${}^{6}A_1 \rightarrow {}^{4}E(D)$, ${}^{4}T_2(D)$, ${}^{4}A_1, {}^{4}E(G)$, and ${}^{4}T_2(G)$ are converted into energy coordinates of 30121, 26667, 24272, and 21834 cm^{-1}, respectively.

1. Supplementary Tables

Table S1. The Crystallographic Data of Complexes R/S-Mn(Binapo)Br$_2$

Compound	S-Mn(Binapo)Br$_2$	R-Mn(Binapo)Br$_2$
Empirical formula	C$_{44}$H$_{32}$Br$_2$MnO$_2$P$_2$	C$_{44}$H$_{32}$Br$_2$MnO$_2$P$_2$
Temperature/ K	100	100
Crystal system	Orthorhombic	Orthorhombic
Space group	$P2_12_12_1$	$P2_12_12_1$
a / Å	12.2709(5)	12.3218(4)
b / Å	15.4159(6)	15.3674(5)
c / Å	20.1625(8)	20.1514(6)
α/deg	90	90
β/deg	90	90
γ/deg	90	90
Volume / Å ^{3}	3814.1(3)	3815.7(2)
Z	4	4
ρ / mg cm^{-3}	1.514	1.513
μ / mm^{-1}	6.350	6.347
Rdiation(λ) / Å	1.54178	1.54178
R$_1$ [a]	0.0499(6162)	0.0238(5025)
wR$_2$ [b]	0.1325(6864)	0.0572(5100)
Flackparameter	0.032(12)	0.037(6)
GOF	1.035	1.061

a) R1 = Σ|F_o−F_c|/ΣF_o,   b) wR2 = Σ[w($F_o{}^2$−$F_c{}^2$)^2]/Σ[w(F_o)^2)]$^{1/2}$

Table S2. Selected bond lengths (Å) and angles (°) of R/S-Mn(Binapo)Br$_2$

Bondlengths	S-Mn(Binapo)Br$_2$	R-Mn(Binapo)Br$_2$
Mn-Br1	2.468(1)	2.4688(8)
Mn-Br2	2.468(1)	2.4710(7)
Mn-O1	2.058(5)	2.057(3)
Mn-O2	2.049(6)	2.044(3)

Bondangles	S-Mn(Binapo)Br$_2$	R-Mn(Binapo)Br$_2$
O1-Mn1-Br1	106.6(2)	106.59(8)
O1-Mn1-Br2	111.8(2)	112.68(8)
O1-Mn1-O2	95.5(2)	94.9(1)
O2-Mn1-Br1	109.3(2)	109.07(8)
O2-Mn1-Br2	107.5(2)	107.83(8)
Br1-Mn1-Br2	122.78(6)	122.30(3)

Table S3. Optimization process for OLED devices

Doping ratio	ETL	V_{on} (V)	L_{max} (cd/m^2)	CE_{max} (cd/A)	PE_{max} (lm/W)	EQE_{max} (%)	EL (nm)
1%S	BmPyPb	4.4	1589	2.38	1.59	1.04	594
2%S	BmPyPb	4.7	1219	4.43	2.56	1.93	593
3%S	BmPyPb	6.0	1145	4.85	2.42	2.11	594
5%S	BmPyPb	4.8	955	4.79	2.12	2.08	594
10%S	BmPyPb	4.4	835	2.82	1.89	1.23	594
20%S	BmPyPb	4.3	649	2.29	1.52	0.99	594
40%S	BmPyPb	4.4	326	0.64	0.45	0.28	602
60%S	BmPyPb	4.8	107	0.45	0.29	0.19	602

Doping ratio	ETL	V_{on} (V)	L_{max} (cd/m^2)	CE_{max} (cd/A)	PE_{max} (lm/W)	EQE_{max} (%)	EL (nm)
100%S	BmPyPb	6.5	31	0.045	0.043	0.022	635

Doping ratio	ETL	V_{on} (V)	L_{max} (cd/m^2)	CE_{max} (cd/A)	PE_{max} (lm/W)	EQE_{max} (%)	EL (nm)
3%S	BmPyPb	4.2	933	4.62	3.29	1.99	593
3%S	TPBi	4.8	2012	2.04	1.28	0.91	589
3%S	TmPyPb	4.2	843	8.79	5.80	4.09	597
3%R	TmPyPb	5.1	791	7.55	4.39	3.24	596

Table S4. Circularly polarized electroluminescence properties of recently reported complexes.

Material	morphological	Dissymmetry Factor (g_{lum})	λPL (nm)	PLQY (%)	λEL (nm)	Dissymmetry Factor (g_{EL})	Ref.
CsEu((±)-hfbc)4	supramolecular aggregates powder	1.41/0.25	586/ 595/ 612/ 652/ 704	3	595/612	0.75/0.15	[1]
Λ/Δ-Ir(dfppy)2(R/S-edp)	crystals	3.3x10^{-3}	606	92	595	4.3x10^{-4}	[2]
bis-cyclometalated Ir(III) isocyanide	Solid	Approximately 0	527/ 558	21	525/557	3x10^{-3}	[3]
mono-platina[6]helicene	crystals	1.3x10^{-2}	644	10	622	0.38	[4]
2-(4-fluorobenzo[c]phenanthren-1-yl)-5-(trifluoromethyl)pyridine	crystals	3.7 x10^{-3}	612	27	≈ 650	5.1x10^{-3}	[5]

		g_{lum}				g_{EL}	
chiral salen-Zn(II) complex enantiomers (R-/S-ZnL)	Solid	3×10^{-3}	576	14.8	576	4.4×10^{-2}	[6]
RP/SP)-CzpPhTrz	crystals	1.3×10^{-3}	470	70	480	-	[7]
(+/-)-(S,S /R,R)-CAI-Cz	Solid	1.1×10^{-3}	533	41	520	2.3×10^{-3}	[8]
R/S-OBN-DPA	crystals	2×10^{-3}	538	84.67	544	2.9×10^{-3}	[9]
R/S-P	polymers	2.1×10^{-3}	659	37	662	1.7×10^{-3}	[10]
R/S-NBCP	perovskite film	2.1×10^{-3}	683	31.5	686	4.0×10^{-3}	[11]
R-BBT2TPA	Solid	2.3×10^{-4}	530/665	99	556	2.0×10^{-3}	[12]
Ir(III)(ppy)3/Ir(III)(ppy)2(acac)	Solid	$(1.2/0.96) \times 10^{-3}$	513/534	-	513/522	$(0.9/0.7) \times 10^{-4}$	[13]
R/S-OBN-(2/4)CN-BN	CP-MR-TADF enantiomers	$(0.91/1.04) \times 10^{-3}$	493/500	99/95	196/508	$(1.43/0.476) \times 10^{-3}$	[14]
R/S-Ax-CN	crystals	3.3×10^{-3}	503	88.6	518	4.4×10^{-3}	[15]
R/S-Mn(Binapo)Br$_2$	crystals	5×10^{-3}	629	11.38	595	8.5×10^{-3}	This Work

Note: "g_{lum}", Photoluminescence asymmetry factor; "g_{EL}", electroluminescence asymmetry factor
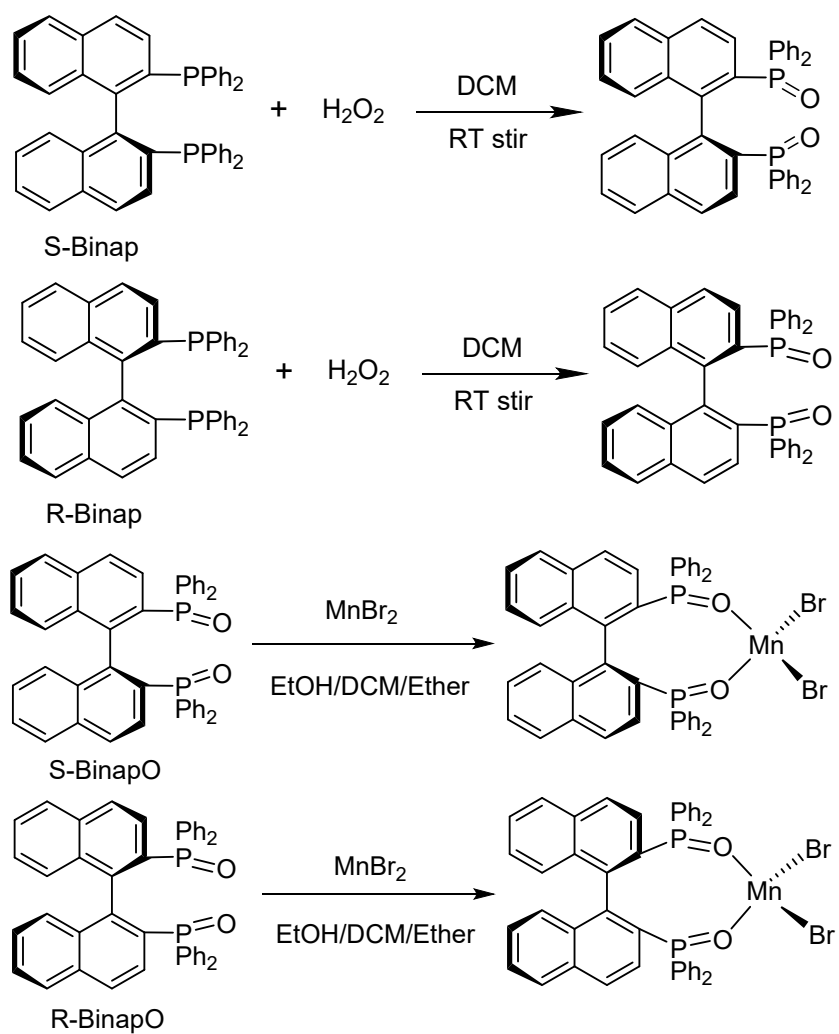
Scheme S1. Synthetic route of the complexes R/S-Mn(Binapo)Br$_2$
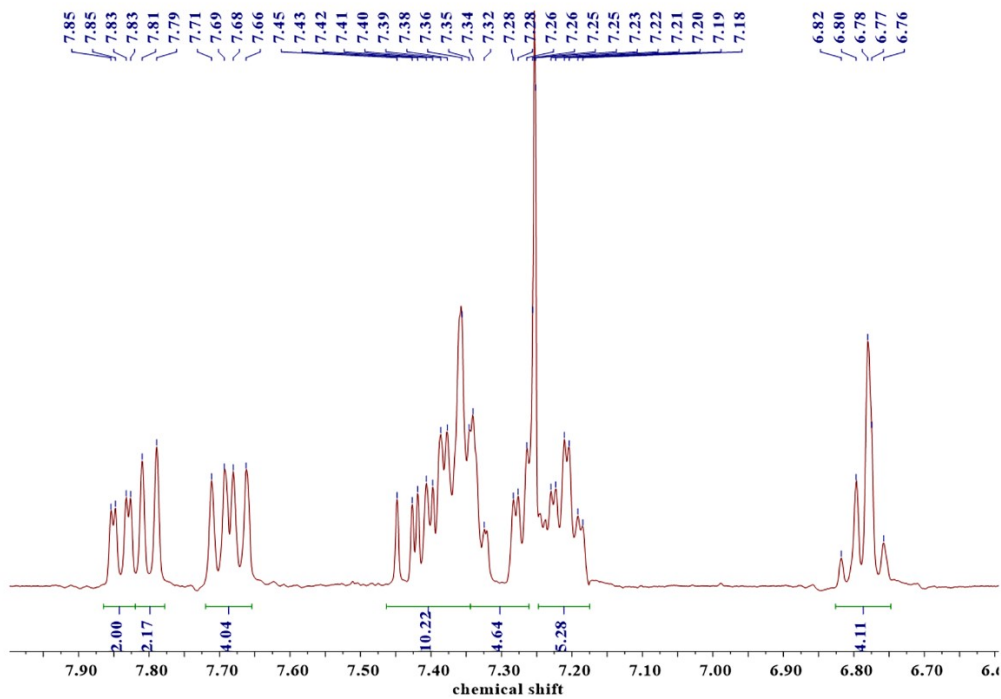
Figure S1. The ^{1}H NMR spectrum of R-Binapo in CDCl${}_3$ solution at ambient temperature.
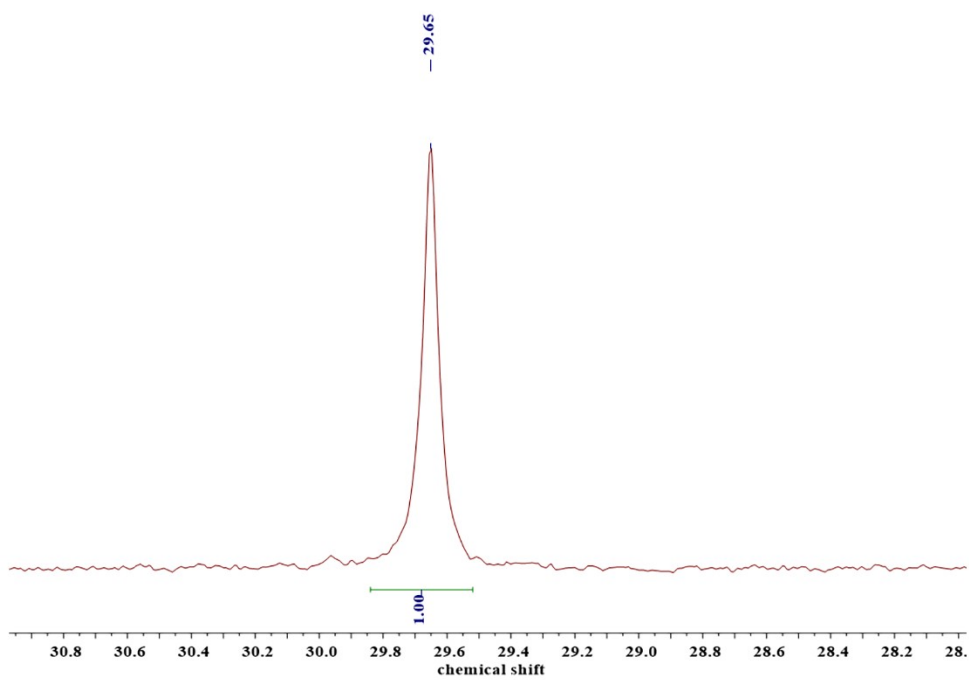
Figure S2. The ^{31}P NMR spectrum of R-Binapo in CDCl${}_3$ solution at ambient temperature.
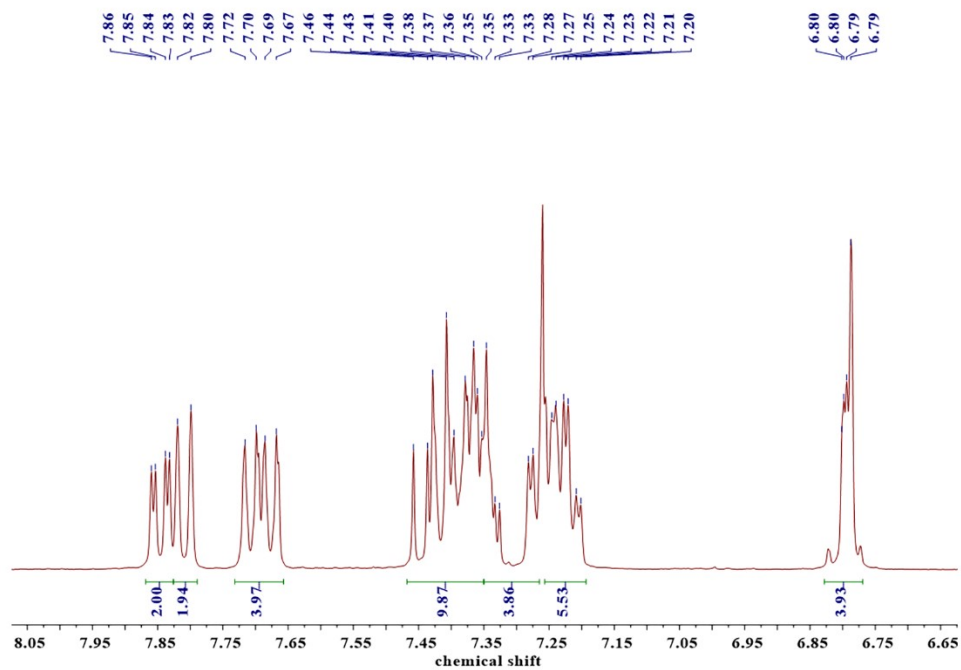
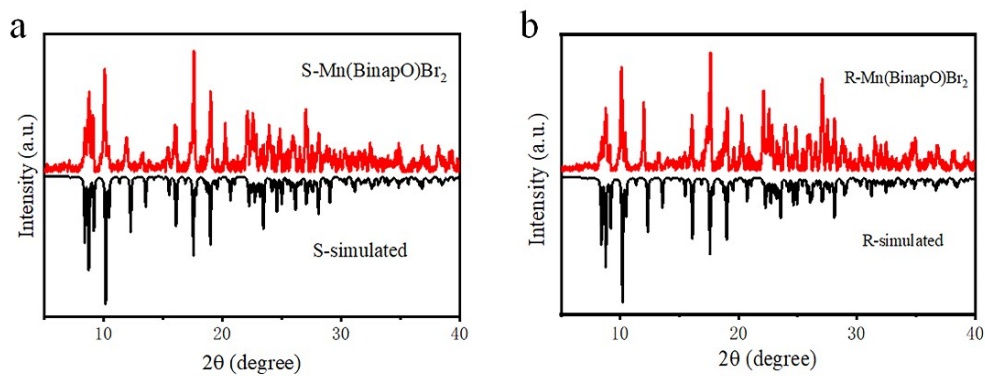**Figure S3.** The ^{1}H NMR spectrum of S-Binapo in CDCl$_3$ solution at ambient temperature.
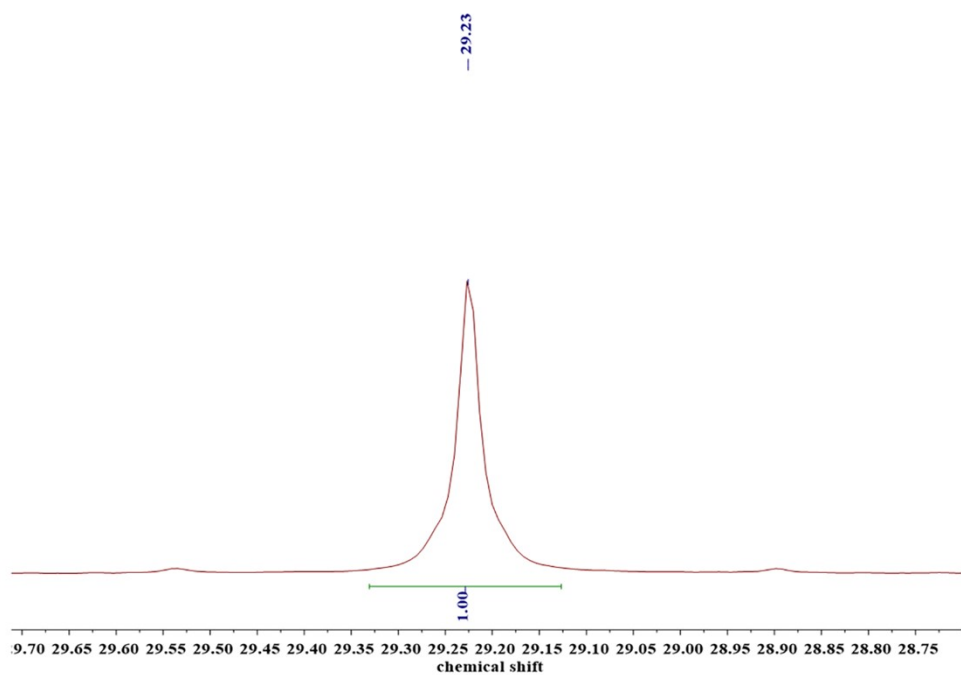
Figure S4. The ^{31}P NMR spectrum of S-Binapo in CDCl$_3$ solution at ambient temperature.
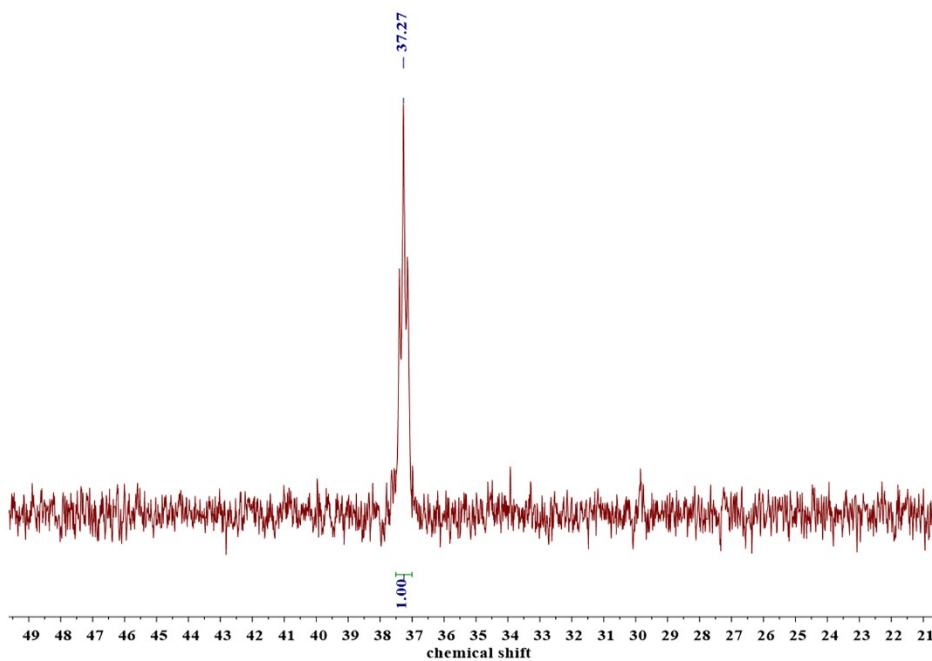
Figure S5. The ^{31}P NMR spectrum of R-Mn(Binapo)Br$_2$ in CDCl$_3$ solution at ambient temperature.
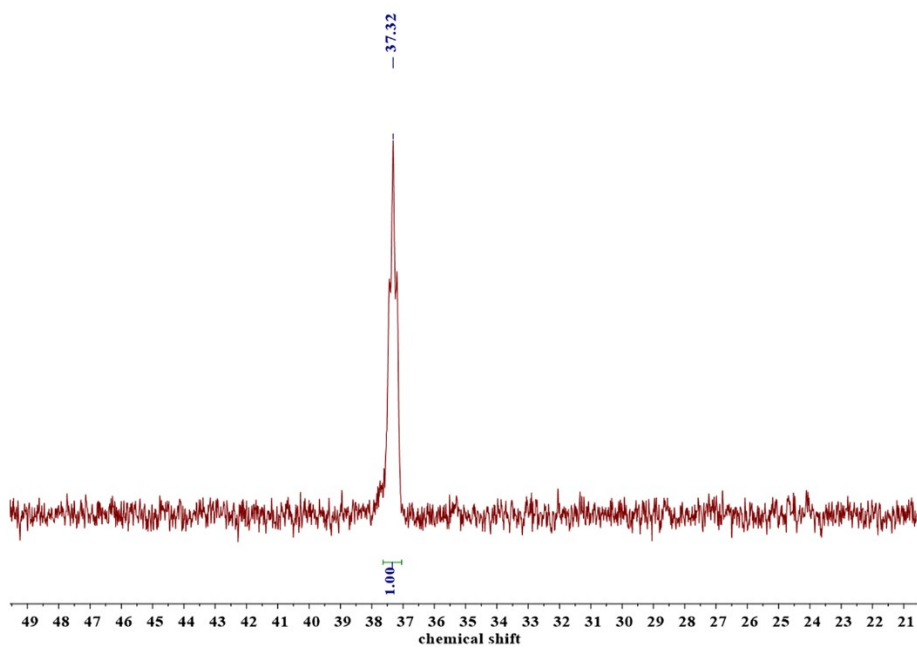
Figure S6. The ^{31}P NMR spectrum of S-Mn(Binapo)Br$_2$ in CDCl$_3$ solution at ambient temperature.

Figure S7. PXRD patterns of R/S-Mn(Binapo)Br$_2$ and the corresponding simulated peaks from crystal structure.
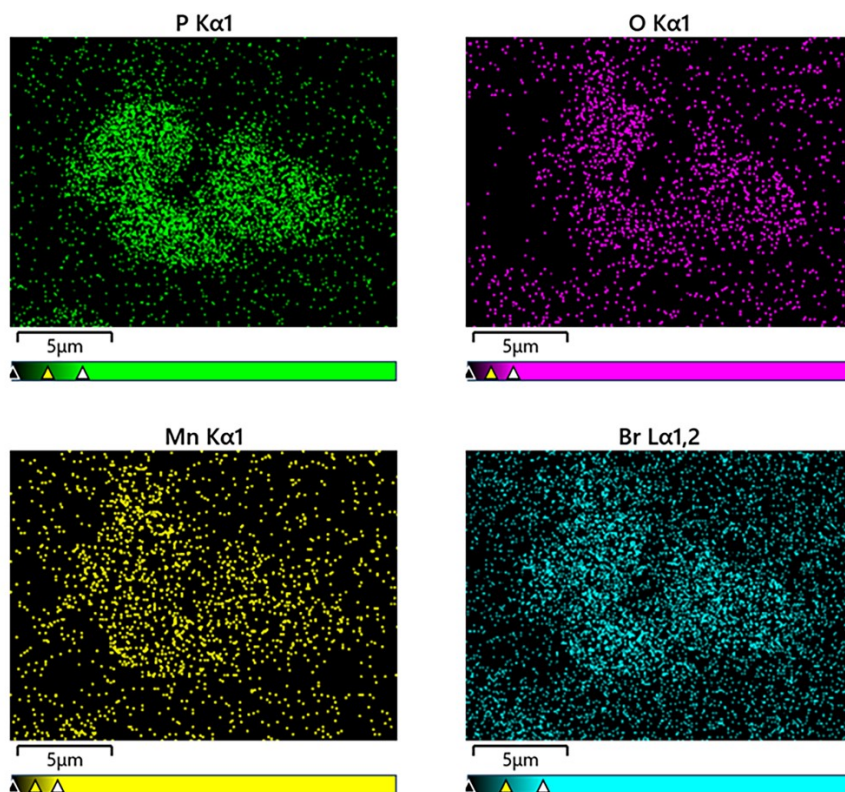
Figure S8. EDS Elemental Spectral Analysis Images of S-Mn(Binapo)Br$_2$
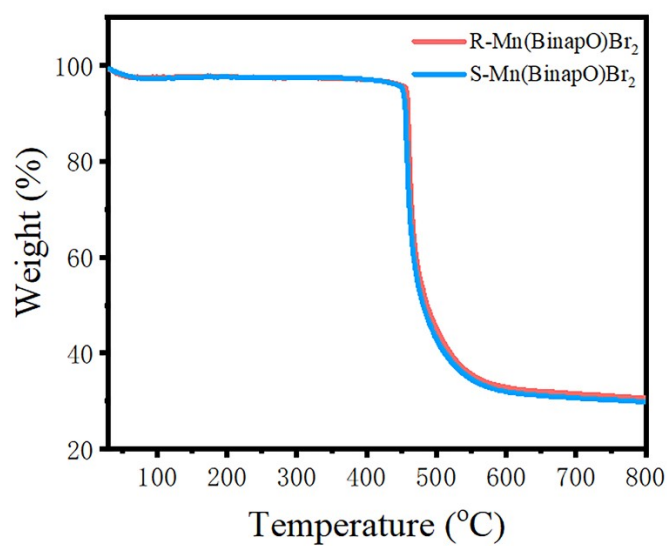
Figure S9. The TGA curve of R/S-Mn(Binapo)Br$_2$.
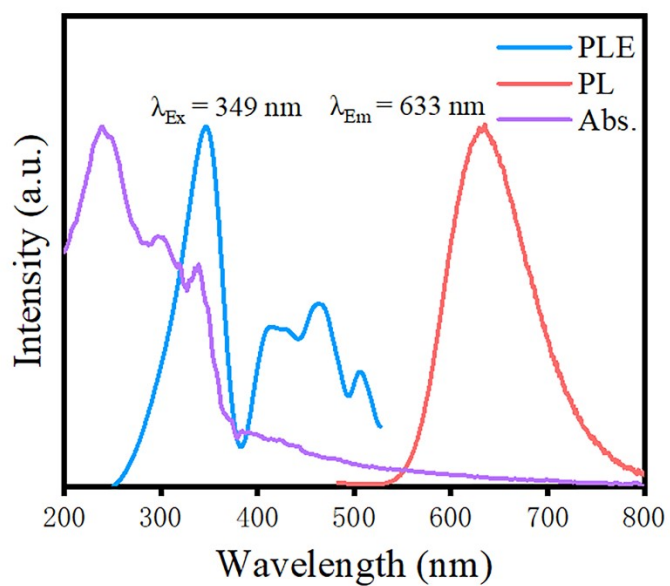
Figure S10. Room-temperature UV absorption and excitation and emission spectrum of R-Mn(Binapo)Br$_2$.
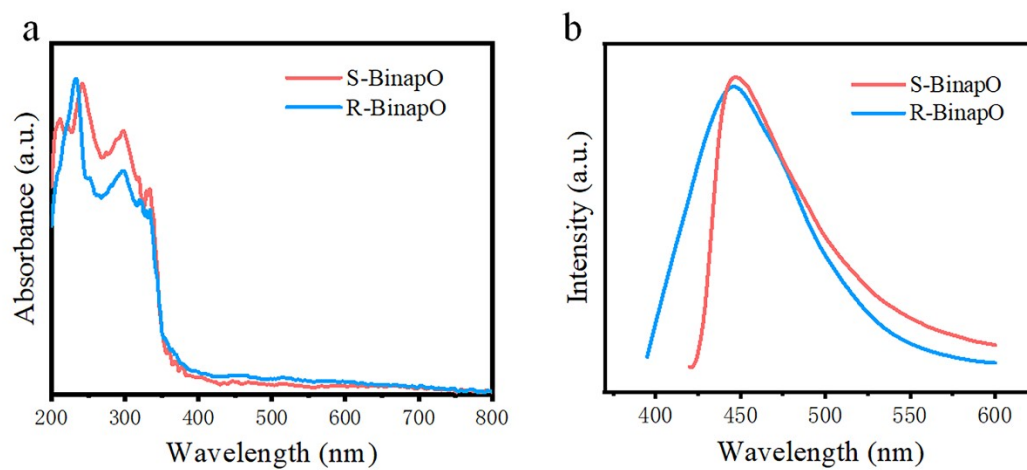
Figure S11. (a) Ultraviolet-visible (UV-Vis) absorption spectra of R/S-Binapo. (b) Emission spectrum of R/S-Binapo.
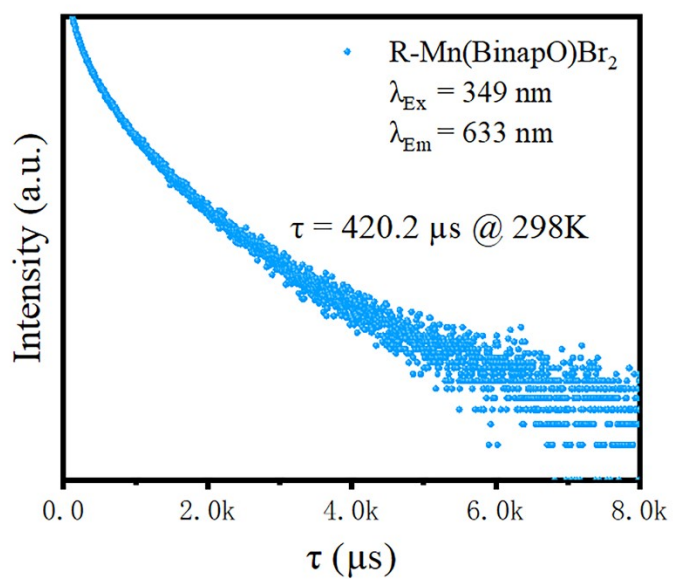
Figure S12. PL decay lifetime curves for R-Mn(Binapo)Br$_2$.
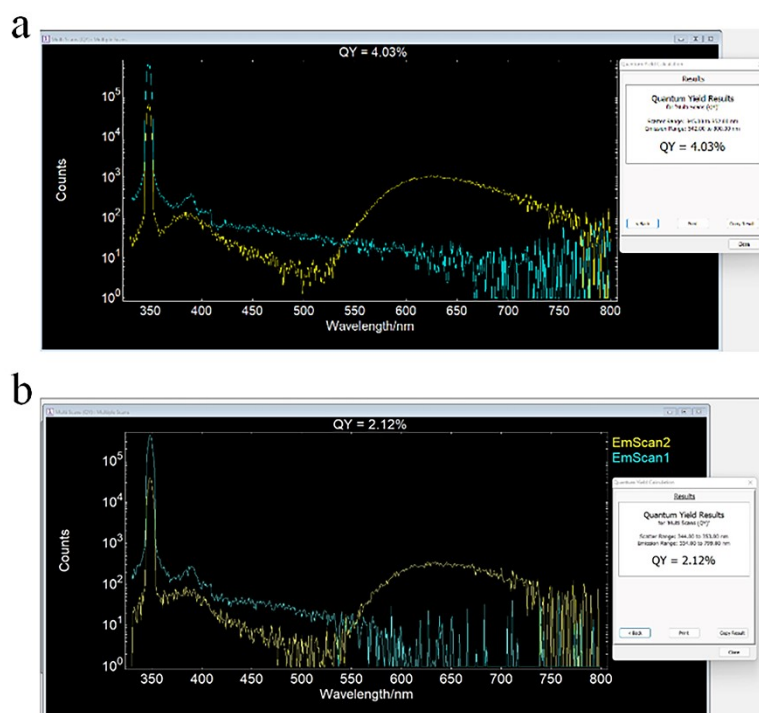
Figure S13. Quantum yield (PLQY) of S-Mn(Binapo)Br$_2$ (a) and R-Mn(Binapo)Br$_2$ (b).
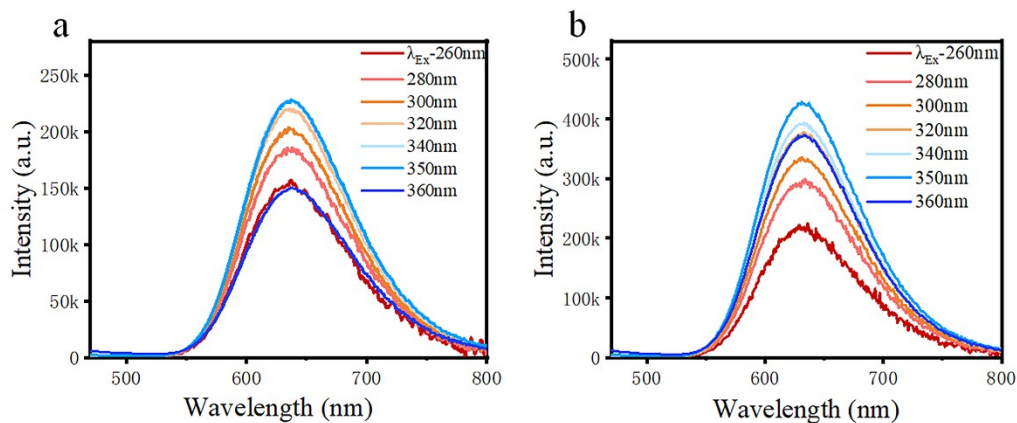
Figure S14. The emission spectra at different excitation wavelengths in the range of 260 to 360 nm for S-Mn(Binapo)Br$_2$(a) and R-Mn(Binapo)Br$_2$(b).
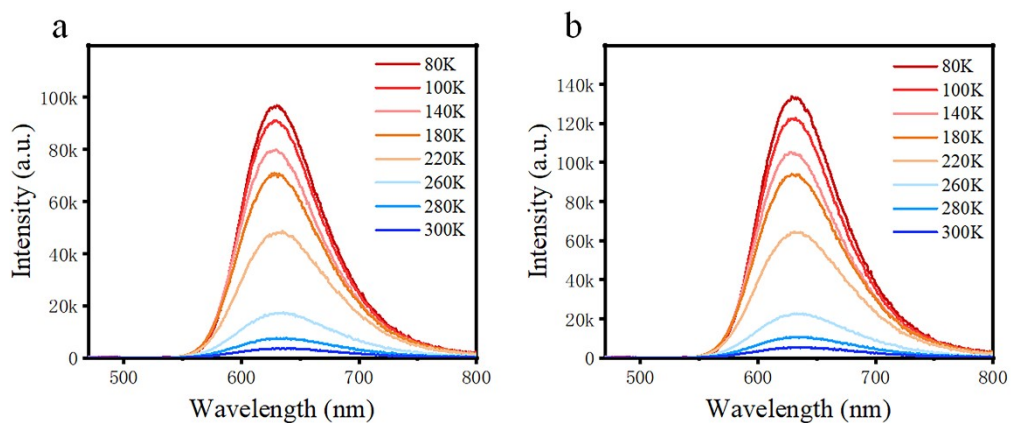
Figure S15. Temperature-dependent emission spectra of S-Mn(Binapo)Br$_2$ (a) and R-Mn(Binapo)Br$_2$ (b).
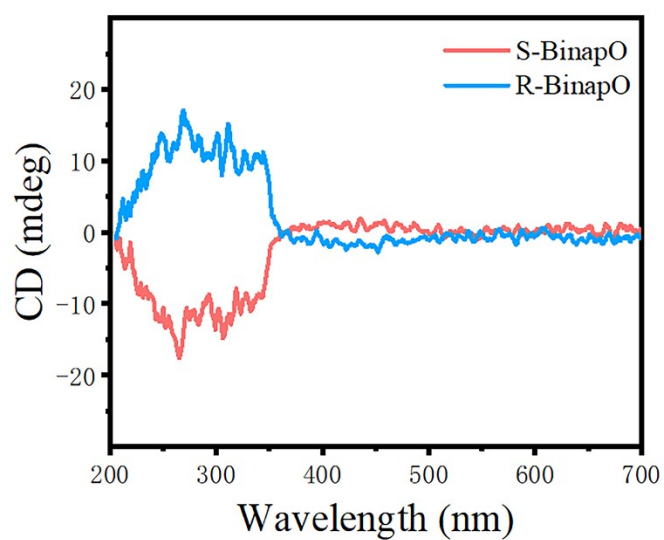
Figure S16. Circular dichroism spectra of R/S-Binapo.
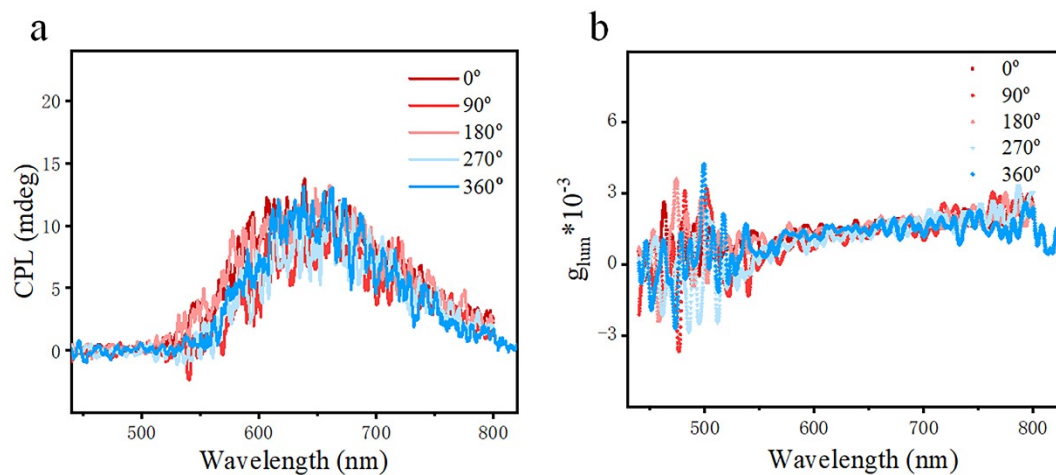
Figure S17. (a) CPL spectra of R-Mn(Binapo)Br$_2$ measured by rotating the sample from 0°~ 360°. (b) Variation of asymmetry factor (g_{lum}) of R-Mn(Binapo)Br$_2$ measured after sample rotation from 0° to 360°.
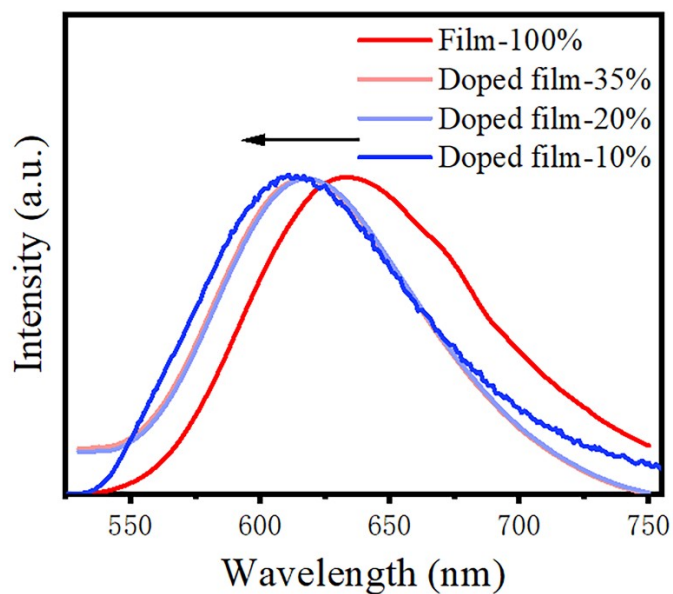

Figure S18. (a) Emission spectrums of S-Mn(Binapo)Br$_2$ and TAPC and 2,6-DCzPPY doped films with different ratios.
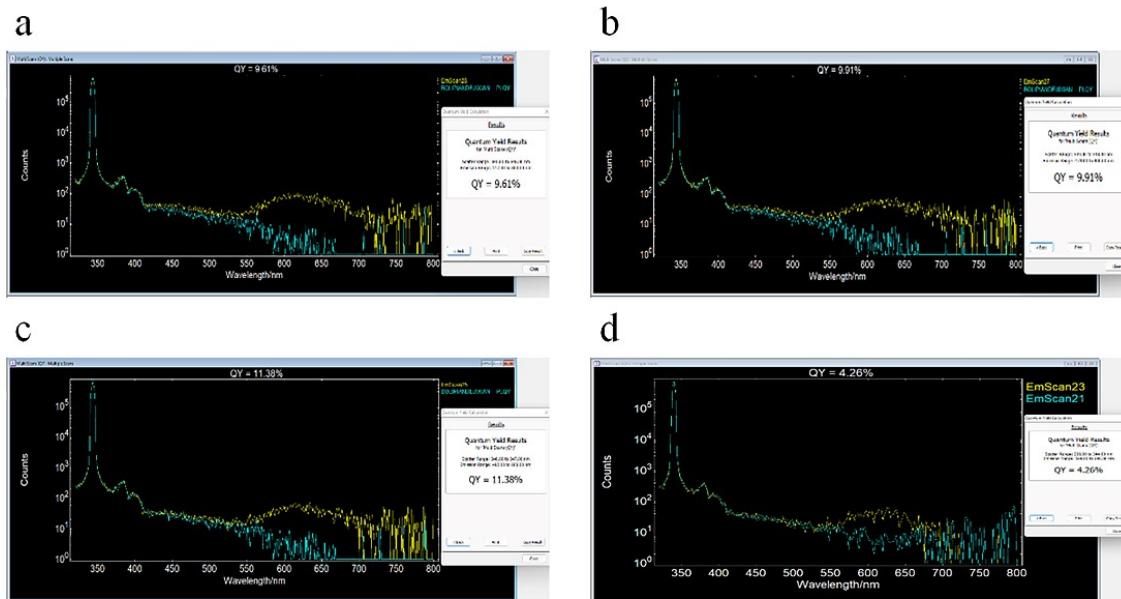
Figure S19. S-Mn(Binapo)Br$_2$ and TAPC and 2,6-DCzPPY doped films with different ratios of PLQY. (a) S-Mn(Binapo)Br$_2$ and TAPC and 2,6-DCzPPY =15:28:57 (b) S-Mn(Binapo)Br$_2$ and TAPC and 2,6-DCzPPY =25:25:50 (c) S-Mn(Binapo)Br$_2$ and TAPC and 2,6-DCzPPY =35:22:43 (d) S-Mn(Binapo)Br$_2$ and TAPC and 2,6-DCzPPY =45:18:37.
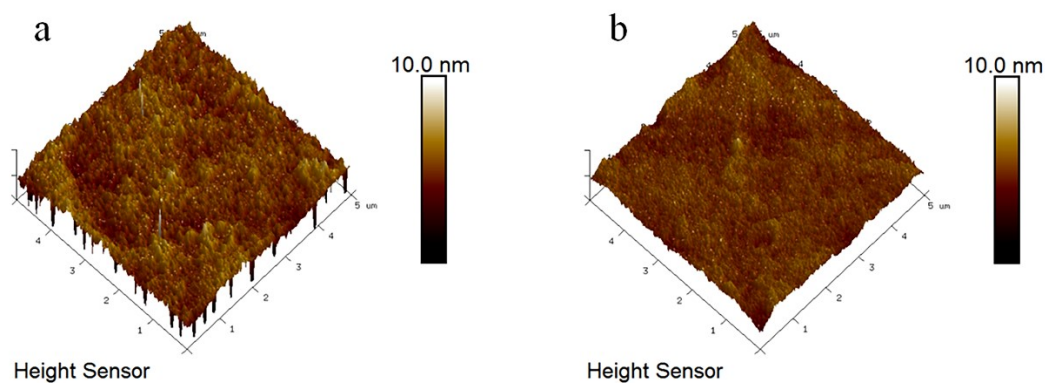

Figure S20. AFM comparison spectrum of non-doped films(a) and doped films(b). and the corresponding root mean square roughness are 1.00 nm and 0.44 nm.
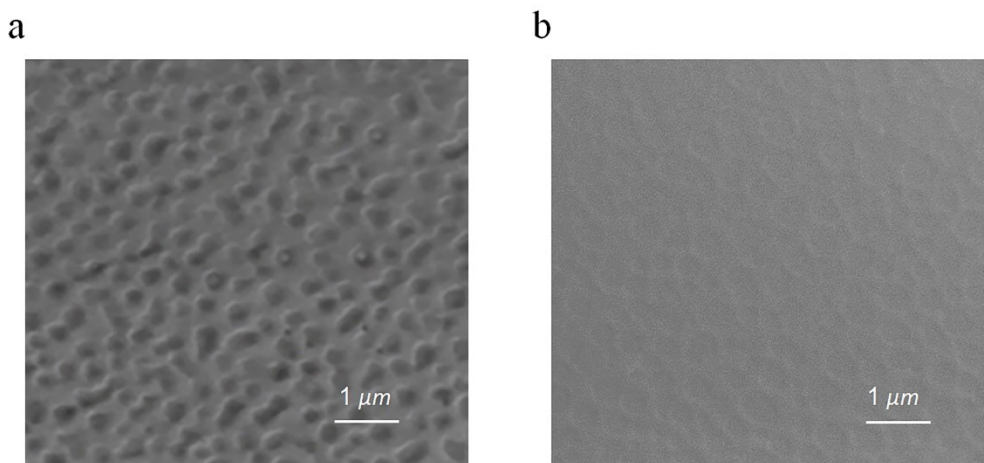
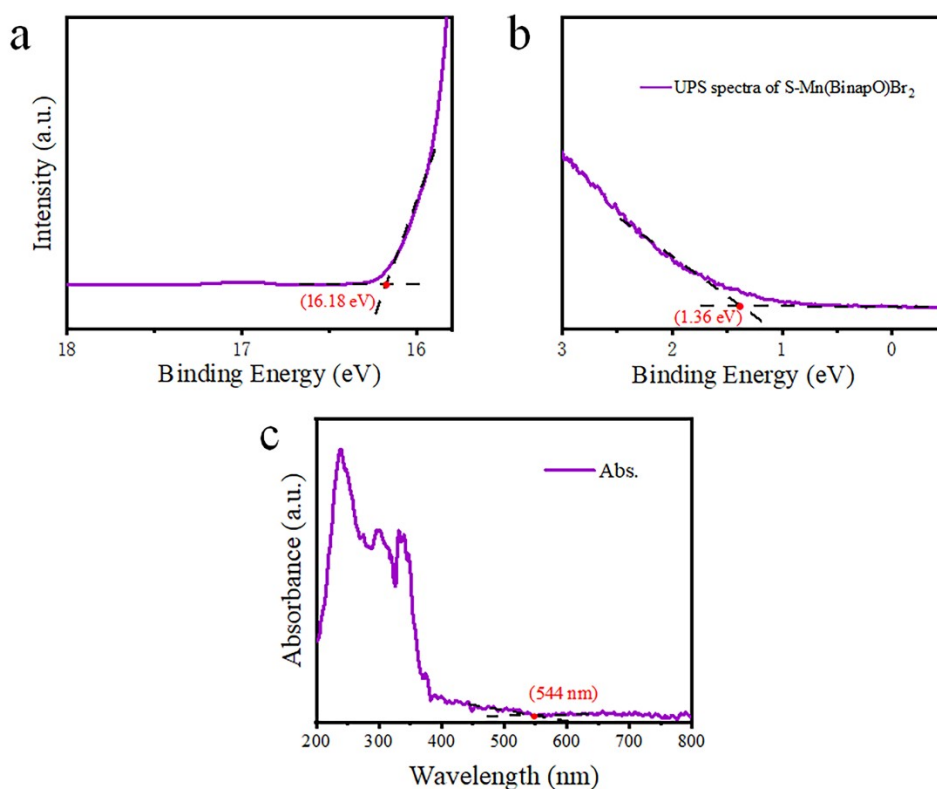**Figure S21.** SEM topography of non-doped films(a) and doped films(b).

Figure S22. The UPS (a, b) and UV-Vis absorption spectra (c) of S-Mn(Binapo)Br$_2$. The HOMO of the S-Mn(Binapo)Br$_2$ could be obtained through the following equation E_{HOMO}=hγ-(E_{cutoff} - E_{onset}), where hγ is the UV photo energy of He excitation source (21.2 eV), and E_{cutoff} is determined by linear extrapolation to zero of the yield of secondary eletrons and the E_{onset} is the onset of the film relative to the EF of Au. Therefore, E_{HOMO} = 21.2 - (16.18 - 1.36) = 6.38 eV. The LUMO energy is calculated using the HOMO levels and the optical gaps (E_g) obtained from UV-Vis absorption spectra. E_{LUMO}=E_{HOMO}-E_g = 6.38 - 1241/ 544 = 4.09 eV.
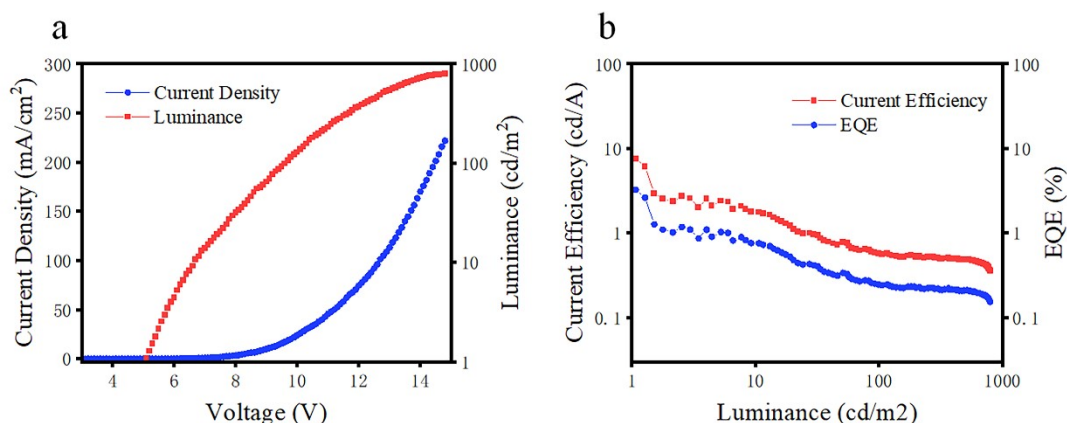
Figure S23. (a) Current density-voltage-luminance (J-V-L) curves of the doped device for R-Mn(Binapo)Br$_2$. (b) Current efficiency-brightness-external quantum efficiency (CE-L-EQE) curve of the dopant device.

Reference

[1]. F. Zinna, U. Giovanella and L. D. Bari, *Adv. Mater.*, 2015, **27**, 1791–1795

[2]. Z.-P. Yan, K. Liao, H.-B. Han, J. Su, Y.-X. Zheng and J.-L. Zuo, *Chem. Commun.*, 2019, **55**, 8215–8218

[3]. J. Han, S. Guo, J. Wang, L. Wei, Y. Zhuang, S. Liu, Q. Zhao, X. Zhang and W. Huang, *Adv. Opt. Mater.*, 2017, **5**, 1700359

[4]. J. R. Brandt, X. Wang, Y. Yang, A. J. Campnell and M. J. Fuchter, *J. Am. Chem. Soc.*, 2016, **138**, 9743–9746

[5]. Z.-P. Yan, X.-F. Luo, W.-Q. Liu, Z.-G. Wu, X. Liang, K. Liao, Y. Wang, Y.-X. Zheng, L. Zhou, J.-L. Zuo, Y. Pan and H. Zhang, *Chem. – Eur. J.*, 2019, **25**, 5672–5676

[6]. Y. Chen, X. Li, N. Li, Y. Quan, Y. Cheng and Y. Tang, *Mater. Chem. Front.*, 2019, **3**, 867–873

[7]. N. Sharma, E. Spuling, C. M. Mattern, W. Li, O. Fuhr, Y. Tsuchiya, C. Adachi, S. Bräse, I. D. W. Samuel and E. Zysman-Colman, *Chem. Sci.*, 2019, **10**, 6689–6696

[8]. M. Li, S. H. Li, D. Zhang, M. Cai, L. Duan, M. K. Fung and C.-F. Chen, *Angew. Chem., Int. Ed.*, 2018, **57**, 2889–2893

[9]. Z.-G. Wu, Z.-P. Yan, X.-F. Luo, L. Yuan, W.-Q. Liang, Y. Wang, Y.-X. Zheng, J.-L. Zuo and Y. Pan, *J. Mater. Chem. C*, 2019, **7**, 7045–7052

[10]. J.-M. Teng, C.-F. Chen. *Adv. Opt. Mater.*, 2023: 2300550.

[11]. C.-H. Yang, S.-B. Xiao, H. Xiao, L.-J. Xu and Z.-N. Chen, *ACS Nano*, 2023, 17(8): 7830-

7836.

[12]. F.-C. Kong, S.-Y. Yang, X.-J. Liao, Z.-Q. Feng, W.-S. Shen, Z.-Q. Jiang, D.-Y. Zhou, Y.-X. Zheng and L.-S. Liao, *Adv. Func. Mater.*, 2022, **32**: 2201512.

[13]. Hara K, Morimoto A, Matsudaira K, Suzuki S, Yagi S, Fujiki M, and Imai, Y, *ChemPhotoChem*, 2022, 6(4): e202100253.

[14]. Y.-C. Xu, Q.-Y. Wang, X.-L. Cai, C.-L. Li and Y Wang, *Adv. Mater.*, 2021, 33(21): 2100652.

[15]. K.-K. Tan, D.-W. Zhang, W.-L. Zhao, M Li and C.-F. Chen, *Chem. Eng. J.*, 2023, 462: 142123.